Intralaminar Damage Model for Laminates subjected to Membrane and Flexural Deformations

Adi Adumitroaie[1] and E. J. Barbero[2]

Mechanical and Aerospace Engineering, West Virginia University, Morgantown, WV 26506-6106, USA

Abstract

Prediction of transverse damage initiation and evolution for not necessarily symmetric laminates under membrane and/or bending loads is the subject of this work. The laminate stiffness reduction is computed via crack opening displacement (COD) methods and the generalization to multiple cracking laminas is made via continuum damage mechanics (CDM) concepts. Using available COD solutions combined with homogenization techniques leads to an analytical constitutive model capable of predicting the initiation and evolution of crack density vs. applied strain, as well as laminate modulus degradation, not only for symmetric laminates subjected to membrane deformation but also for general laminates subjected to flexural deformations as well. To adjust the model parameters, experimental data is required in the form of crack density, or modulus reduction, vs. strain for two laminates of the same material system. Then, the model is capable of predicting crack density and modulus degradation for other laminate stacking sequences. The model takes into account crack closure, which is important under flexure, as well as the case of the center lamina straddling the neutral axis. The effect of thermal stresses is incorporated in the formulation.

Keywords

Damage, Membrane, Flexural, Toughness, Unsymmetric

1 Introduction

The problem of transverse matrix cracking in laminated composites has been extensively studied for the particular case of symmetric $[0_m/90_n]_S$ laminates under membrane loads, for which matrix cracking is found in the 90° laminas (transverse laminas). Extensions to other laminate configurations such as $[0/\pm\theta/0]_S$ and $[0/\theta_1/\theta_2]_S$, models featuring cracks in the off-axis θ laminas have been developed, but they are still limited to *symmetric laminates* under *in-plane loading*. In con-

---

[1]Graduate Research Assistant.

trast, the general case of a $[\theta_1/\theta_2/\ldots/\theta_n]$ laminate with matrix cracks with multiple laminas under general membrane and flexural loading, is the subject of this work.

Continuum Damage Mechanics (CDM) models homogenize the cracks [1–7]. That is, they calculate the degraded moduli of the laminas and laminate in terms of continuum damage variables. Either strength or fracture mechanics failure criteria are used to detect damage initiation. Then, damage evolution is predicted in terms of phenomenological equations set up in terms of additional parameters. From a thermodynamics point of view, damage variables are the state variables of the formulation. From a practical point of view, CDM major shortcoming is the need for additional experimentation to determine parameters that are particular to each model.

Micromechanics of Damage Models (MMD) find an approximate elasticity solution for a laminate with a discrete crack or cracks [8–29]. The solutions are approximate because kinematic assumptions are made, such as a linear [30] or bilinear [31] distribution of interlaminar shear stress through the thickness of each lamina, as well as particular spatial distributions of inplane displacement functions [28], stresses, and so on. The state variable is the crack density. One advantage of MMD is that the the reduction of laminate moduli as a function of crack density is calculated without resorting to additional parameters as in the case of CDM. Still, additional parameters may be required to deal with R-curve behavior. The main disadvantage of MMD is that most of the solutions available are limited to *symmetric laminates under membrane loads*.

Crack Opening Displacement (COD) models [32–39] are based on the theory of elastic bodies with voids [40]. The main advantage of COD models is that the laminate stiffness can be calculated for any laminate configuration, even non-symmetric laminate stacking sequence (LSS), subject to any deformation, including bending, featuring matrix cracking in any of its laminas. Based on this distinctive advantage, the reduced stiffness analytical model in [35] is used in the present work in order to implement the model of the progressive damage matrix cracking in general LSS laminates.

Numerical solutions, such as FEA, provide 3D solutions without the kinematic simplifications of MMD and COD models [19, 35, 38, 41–43]. However, FEA solutions require a new mesh and boundary conditions for each LSS, crack orientation, and so on, making them too cumbersome for practical application. Another numerical approach is Monte Carlo simulation, where the probabilistic distribution of flaws in material is considered [4, 6, 44]. Unfortunately, Monte Carlo simulations require additional parameters that have to be adjusted by fitting the results of the model to the damage evolution data obtained experimentally. Such data is scarce.

Synergistic Damage Mechanics (SDM) models combine elements of different modeling strategies such as CDM and MMD [3, 4, 6, 45, 46], bringing the best features of each of the models involved. The present work is in this category. That is, the laminate stiffness reduction is computed via COD methods and the generalization to multiple cracking laminas is made via CDM concepts, but unlike CDM models, no additional parameters are needed.

Models addressing flexural deformations are scarce and limited in applicability. A 1D beam bending model for $[0/90]_S$–like laminates where only one of the $90°$ laminas is allowed to crack is offered in [47, 48]. The plane stress assumption in [49] restricts the flexural analysis to $[0_m/90_n]_S$ laminates with cracks developing only in the $90°$ center lamina. The finite strip solution in [3, 50] relies on the generalized plane strain assumption. To satisfy this assumption, all the cracking laminas must have the same orientation and same crack density, which is unrealistic under bending unless there is only one cracking lamina. The formulation in [4] uses the model in [50], which in turn relies on the generalized plain strain assumption, thus introducing restrictions about the number and orientation of cracking laminas.

A general LSS damage growth model including flexural deformation in developed in [36]. However, due to the complex phenomenon of the ply thickness dependent R-curve behavior in laminated composites, an energy release based damage evolution law was claimed to be inappropriate [36].

In [36], the proposed alternate damage evolution law relies heavily on experimentation and cannot capture the experimentally observed ply thickness effect (insitu effect) on damage onset. Moreover, the damage law is based exclusively on mode I experimental results, this being the reason the model performs poorly when when mixed modes conditions result in matrix cracking in off-axis plies.

The objective of this work is to develop an analytical model of progressive damage in form of matrix cracking in general LSS laminates subjected to general membrane and flexural deformation. Both aspects of matrix cracking onset and evolution under external loading are addressed. The process of matrix cracking under I, II, and mixed I-II modes conditions are included in the present model. The loading case can be in-plane, flexural, or combination of the two. The effect of thermal residual stresses and the experimentally observed in-situ and R-curve behaviors of fracture toughness for laminated composites are included in the present model. There is no limitation on the configuration of the laminate, on the number of the cracking plies, or on the type of loading (membrane, flexural, or both) as it is the case for the most models available in the literature.

The proposed constitutive model is currently implemented as a stand alone program capable of predicting initiation and evolution of damage at a single location (x, y) in a laminate, which is loaded by membrane and/or bending stress resultants. The proposed model could be implemented into a finite element program in order to solve boundary value problems of laminated shells but that falls outside the scope of this work.

2 Laminate Stiffness

In this work, the laminate stiffness as a function of crack densities in the various laminas is calculated using the crack opening displacement (COD) model in [35], which defines crack density as $\rho^{(k)} = t^{(k)}/d$, where $t^{(k)}$ is the thickness of the cracking lamina and d is the distance between two adjacent cracks.

The COD is defined as the average relative displacement between two faces of the same crack lying along the fiber direction of a lamina

$$\Delta u_i^{(k)} = \frac{1}{t^{(k)}} \int_0^{t^{(k)}} \left[u_i^{(k)(+)}(z) - u_i^{(k)(-)}(z) \right] \, dz \tag{1}$$

where the $u_i^{(k)(+)}(z), u_i^{(k)(-)}(z)$, are the displacements of opposite surfaces of the crack in lamina coordinate system (c.s.).

Since the COD are affected by the laminate stacking sequence (LSS), a generalization of analytical COD solutions for general laminate configurations has yet to be found. Thus, COD solutions are approximated by either i) equations designed to fit the results of parametric FEA simulations [32, 35, 39], or ii) extensions of the fracture mechanics solution for similar problems [32–35]. The latter uses FEA to asses the level of error of the solution to the problem of laminated composite with cracked laminas. For both cases, the COD in lamina k can be written `empirically` as a linear combination of the surface tractions $\tau^{(l)}$ at the laminas l times the COD compliances $\beta_{ij}^{(kl)}$, as follows

$$\Delta u_i^{(k)} = t^{(k)} \sum_{l=1}^{N} \beta_{ij}^{(kl)} \tau_j^{(l)} \quad ; \quad i, j = 1 \ldots 3 \tag{2}$$

where N is the total number of plies inside of the laminate.

The COD compliances $\beta_{ij}^{(kl)}$ quantify the effect of traction in lamina l on the COD in lamina k. The formulation can be simplified introducing uncoupling [35], i.e., $\beta_{ij}^{(k)} = \beta_{ij}^{(kl)} \delta_{kl}$, where δ_{kl}

is the Kronecker symbol. That is, the COD in lamina k only depends on the traction in lamina k. The lamina tractions $\tau_j^{(l)}$ are computed using Classical Lamination Theory (CLT) on the intact laminate.

For a given crack density array $\{\rho\}$ representing the crack density in all the laminas, the laminate A, B, and D matrices of the undegraded (intact) laminate are updated as follows

$$\begin{bmatrix} A & B \\ B & D \end{bmatrix}^{(\rho)} = \begin{bmatrix} A & B \\ B & D \end{bmatrix} - \begin{bmatrix} \Delta A & \Delta B \\ \Delta B & \Delta D \end{bmatrix} \tag{3}$$

where the reduction (degradation) of the membrane, bending-extension, and bending matrices is given by [35]

$$\Delta A = \sum_{j=1}^{N} t^{(k)} \rho^{(k)} A_{EE}^{(k)}$$

$$\Delta B = \sum_{j=1}^{N} t^{(k)} \rho^{(k)} \left[z^{(k)} A_{EE}^{(k)} + \frac{1}{2} t^{(k)} A_{BE}^{(k)} \right]$$

$$\Delta D = \sum_{j=1}^{N} t^{(k)} \rho^{(k)} \left[(z^{(k)})^2 A_{EE}^{(k)} + z^{(k)} t^{(k)} A_{BE}^{(k)} + \frac{1}{4} (t^{(k)})^2 A_{BB}^{(k)} \right] \tag{4}$$

The 3×3 matrices $A_m^{(k)}$ for lamina k are computed as

$$A_m^{(k)} = \overline{Q}^{(k)} (R^{(k)})' \beta_m^{(k)} R^{(k)} \overline{Q}^{(k)} \tag{5}$$

where $m = EE, BE, BB$, denote extension, bending-extension, and bending, respectively; $()'$ denote the transpose of a matrix, and $\overline{Q}^{(k)}$ is the undamaged lamina stiffness in laminate c.s. The $R^{(k)}$ matrices are transformation matrices from lamina k to laminate c.s., as follows

$$R^{(k)} = \begin{pmatrix} n_1^{(k)} & 0 & n_2^{(k)} \\ 0 & n_2^{(k)} & n_1^{(k)} \end{pmatrix} \tag{6}$$

where $n_1^{(k)}, n_2^{(k)}$, are the direction cosines between lamina k coordinate system (c.s.) and laminate c.s.

The COD compliances are given in [35] for the various cases including interior and exterior cracks, extension and bending deformation, as well as mode I (`opening`) and mode II (`shear,` but called mode III in [35]), as follows

Interior cracks :

    – Extension:

      - Mode I

$$\beta^k = \frac{\pi}{2} \gamma_2^k \sum_{j=1}^{10} \frac{a_j}{(1 + \rho^k)^j}$$

      - Mode II

$$\beta^k = \frac{\pi}{2} \gamma_1^k \frac{8}{(\pi \rho^k)^2} ln \left[cosh \left(\frac{\pi \rho^k}{2} \right) \right]$$

– Bending:

- Mode I

$$\beta^k = \frac{\pi}{16}\gamma_2^k \sum_{j=1}^{10} \frac{c_j}{(1+\rho^k)^j}$$

- Mode II

$$\beta^k = \frac{\pi}{16}\gamma_1^k \sum_{j=1}^{10} \frac{b_j}{(1+\rho^k)^j}$$

Surface cracks :

– Extension:

- Mode I

$$\beta^k = 1.1215^2\pi\gamma_2^k \sum_{j=1}^{10} \frac{d_j}{(1+\rho^k)^j}$$

- Mode II

$$\beta^k = \pi\gamma_1^k \frac{8}{(2\pi\rho^k)^2} ln \left[cosh\left(\pi\rho^k\right)\right]$$

– Bending-extension coupling:

- Mode I

$$\beta^k = -0.2364\pi\gamma_2^k \sum_{j=1}^{10} \frac{f_j}{(1+\rho^k)^j}$$

- Mode II

$$\beta^k = -\frac{3\pi-8}{3}\gamma_1^k \sum_{j=1}^{10} \frac{e_j}{(1+\rho^k)^j}$$

– Bending:

- Mode I

$$\beta^k = 0.1481\pi\gamma_2^k \sum_{j=1}^{10} \frac{h_j}{(1+\rho^k)^j}$$

- Mode II

$$\beta^k = \frac{3\pi^2-16\pi+24}{3\pi}\gamma_1^k \sum_{j=1}^{10} \frac{g_j}{(1+\rho^k)^j}$$

where the coefficients γ_1, γ_2, are function of transversely isotropic material properties of the lamina, i.e., $\gamma_1 = 1/(2G_{TL})$ and $\gamma_2 = (1 - \nu_{LT}\nu_{TL})/E_T$.

The values of the coefficients $a_j, b_j, c_j, d_j, e_j, f_j, g_j, h_j$ represent numerical integration constants, which are tabulated in [35,36], and $\beta^{(k)} = 0$ for bending–extension coupling with interior cracks [35].

3   Lamina Stiffness

The degraded stiffness of the lamina are calculated by taking into account that at each step of the solution, only lamina (c) is cracking and the remaining laminas are already homogenized using

a previously converged crack density in those laminas. Therefore, the reduced properties of the cracking lamina are computed as follows [46, (21)]

$$Q^{(c)} = \frac{1}{t^{(c)}} \left[A^{(c)} - \sum_{k=1}^{N} (1 - \delta_{k,c}) t^{(k)} Q^{(k)} \right] \tag{7}$$

where $A^{(c)}$ is the degraded laminate in-plane stiffness matrix calculated with (3) when lamina (c) is cracking and the remaining laminas are homogenized from a previous step. The degraded lamina stiffness is saved so that it can be used in subsequent steps.

4　Damage Initiation and Evolution

Two main methodologies are available for damage initiation: strength based [3, 4, 51], and energy based [8, 10, 17, 18, 21–23, 25, 26, 45, 46, 51–53]. The following equation

$$g = (1 - r)\sqrt{\frac{G_I}{G_{Ic}}} + r\frac{G_I}{G_{Ic}} + \frac{G_{II}}{G_{IIc}} - 1 \le 0 \quad ; \quad r = \frac{G_{Ic}}{G_{IIc}} \tag{8}$$

was proposed in [18] as a failure criteria, and its applicability has been extended to damage evolution criteria in [45,46]. G_I, G_{II}, are laminate energy release rates due to opening mode I and shear mode II [54, Fig. 10.4], and G_{Ic}, G_{IIc}, are critical energy release rates in mode I and II, i.e., material properties of the laminate. The material remains undamaged as long as $g \le 0$. With (8) casted in this way, standard tools from plasticity theory, such as the return mapping algorithm, can be used to find the damage level that maintains the material point in equilibrium while simultaneously satisfying the condition $g = 0$. Since G_I, G_{II}, are monotonically decreasing functions of crack density, due to the concomitant reduction of stiffness, (8) provides automatic hardening in the *crack density vs. strain* space, where the state variable 'crack density' and the thermodynamic force 'strain' are thermodynamically conjugate. Comparison with experimental data in [45,46,55,56] supports the use of this measure of hardening.

For damage evolution, the strength based initiation criteria are usually complemented by phenomenological hardening equations [7], thus requiring additional adjustable parameters. Also, strength based initiation criteria can be complemented by energy based evolution [57], but in this case two sets of materials properties (strength and critical energy release rates) are required. On the other hand, the energy based initiation criteria (8) can be used for damage evolution as well [45,46]. This later option does not require separate material properties to detect damage initiation and to follow damage evolution. Also, it does not require additional adjustable parameters such as those used in the hardening equations. Lastly, unlike strength criteria, energy criteria automatically take into account insitu strength [1, 21, 22, 51]; although energy criteria regularize the transition thickness [58], [59, §7.2.1]. Due to to these advantages, (8) is used in this work for both, initiation and evolution criteria.

Taking into account that transverse cracks are discrete, i.e., they propagate suddenly through the thickness and along the fiber direction [59, §7.2.1], the energy release rates (ERR) in mode I and II are calculated as

$$G_i = -\frac{\Delta U_i}{\Delta A} \tag{9}$$

where ΔU_i, with $i = I, II$, are the changes in strain energy of the laminate due to a new (proposed) crack in lamina (c), and ΔA is the area of the new (proposed) crack, calculated with (14). The proposed crack is used to test whether or not (8) is satisfied.

Since intralaminar cracks may propagate in mode I (opening) and mode II (shearing), the ERR (9) needs to be decomposed into G_I and G_{II}. This is accomplished by writing all the quantities involved in the c.s. of the cracking lamina (c). Then, G_I is calculated with $\varepsilon = \{0, \varepsilon_{22}, 0\}$ and G_{II} is calculated with $\varepsilon = \{0, 0, \varepsilon_{12}\}$ [25]. The proposed mode separation is consistent with the method of mechanical work during crack closure in classical fracture mechanics [60, (16)], which is the basis for the Virtual Crack Closure Technique (VCCT) in FEA.

When subject to both membrane tractions and bending moments, the strain at the midsurface of lamina k, located at coordinate $z^{(k)}$, is

$$\varepsilon^{(k)} = \varepsilon^0 + z^{(k)}\kappa \tag{10}$$

where ε^0 is the membrane strain and κ is the curvature of the laminate. The total membrane strain and curvature are the sum of a mechanical component, due to the applied traction and bending, plus a thermal component, due to the shrinkage from processing at the stress free temperature (SFT) to room temperature ambient (RTA), i.e.,

$$\varepsilon^{(k)tot} = \varepsilon^{0M} + \alpha\Delta T + z^{(k)}\left(\kappa^M + \kappa^T\right) \tag{11}$$

were α is the coefficient of thermal expansion (CTE) of the laminate and $\Delta T = RTA - SFT < 0$. This expression of $\Delta T < 0$ holds for the case of material processing at high temperature SFT, and matrix cracking experiments performed at the room temperature RTA. However, the analytical model works for any combination of processing and operating temperatures, for example the case of material processing at room temperature and operating at high temperature, for which $\Delta T > 0$.

Experimental data usually reports ε^{exp} as either the applied mechanical membrane strain ε^{0M} for extension experiments, or the applied mechanical curvature κ^M. The reported experimental data ε^{exp} usually includes only one component of the 6×1 mechanical deformation $\varepsilon^M = \{\varepsilon_x^0, \varepsilon_y^0, \varepsilon_{xy}^0, \kappa_x, \kappa_y, \kappa_{xy}\}^M$, either extension or bending. The other 5 components are calculated by the program according to the boundary conditions of the experiment. For more complex experiments, such as biaxial extension, two components of strain, say $\varepsilon_x, \varepsilon_y$, could be reported simultaneously. In any case, the remaining components are calculated by the model according to the boundary conditions of the experimental setup.

Due to CTE mismatch between laminas, only part of the lamina strain in 11 is involved in the strain energy

$$\varepsilon^{(k)} = \left(\varepsilon^{0M} + \alpha\Delta T - \alpha^{(k)}\Delta T\right) + z^{(k)}\left(\kappa^M + \kappa^T\right) \tag{12}$$

were $\alpha^{(k)}$ is the CTE of lamina (k). Then, the strain energy of lamina (k) is

$$U^{(k)} = \frac{S_0}{2} \int_0^{t^{(k)}} \varepsilon^{(k)}\, \overline{Q}^{(k)}\, \varepsilon^{(k)}\, dV \tag{13}$$

where $\overline{Q}^{(k)}$ is the lamina stiffness. Both stiffness and strain are set in the c.s. of the cracking lamina (c) to allow for mode decomposition of the ERR. For each crack density set $\rho = \{\rho^{(1)}, ..., \rho^{(k)}, ..., \rho^{(N)}\}$, the $\overline{Q}^{(c)}$ of the cracking lamina is calculated by (7). For the remaining lamina, $k \neq c$, the $\overline{Q}^{(k)}$ are stored from previous calculation. Lastly, the strain energy of the laminate is calculated as $U = \sum_{k=1}^N U^{(k)}$, and from it the ERR mode I and mode II are computed with (9).

5   Algorithm

The crack density is defined as $\rho^{(k)} = t^{(k)}/d^{(k)}$, where $t^{(k)}$ is the thickness of the cracking lamina and $d^{(k)}$ is the distance between two adjacent cracks. A system of equally spaced matrix cracks in one lamina of a laminate is shown in Fig. 1. The algorithm is started with a very small crack density ρ_0 in each lamina, so that the initial crack spacing d_0 is very large. From the figure, it can be inferred that the total crack length is $l^{(k)} = \sum_i l_i^{(k)}$ and the surface of the laminate is $S = l^{(k)} d^{(k)} = l_0 d_0$.

For each strain (load) step p, the algorithm loops over the N laminas in the laminate, using the damage evolution criterion (8) to test whether of not the addition of one more crack in lamina (c) satisfies the criterion $(g > 0)$ or not $(g \leq 0)$. If it does, it increases the crack density, degrades the lamina stiffness, and tries to add another crack until (8) is no longer satisfied. If more than one lamina cracks during the loop, the program chooses the lamina with higher value of g to become the current cracking lamina (c), then revisits the other laminas.

The number of cracks added to lamina (c) is denoted by i. Therefore, the crack density is $\rho_i = (i+1)\rho_0$, the crack spacing is $d_i = d_0/(i+1)$, the increment in crack density is $\Delta\rho = \rho_0$ for all i, and the increment in crack area is

$$\Delta A = S \, \Delta\rho = S \, \rho_0 \tag{14}$$

Once no further cracks propagate in lamina (c), the program moves to the next lamina. Because of stress redistribution, cracks in one lamina may trigger cracks in another. The program loops repeatedly over the laminas until no more cracks appear at a given load step. Only then the load (strain) is incremented and the program begins again. The result is a data set for crack density vs. strain. Furthermore, modulus vs. strain can be computed by using (3).

6   Crack Closure

Provision has been made to account for crack closure, which is important under flexure. Depending on the sign of the transverse stress, the temporary crack density of the lamina k is chosen according to

$$\rho_i^{(k)} = \begin{cases} (i+1)\rho_0 & \text{if } \sigma_{22}^{(k)} > 0 \quad ; \text{ crack is active} \\ 0 & \text{if } \sigma_{22}^{(k)} \leq 0 \quad ; \text{ crack is passive} \end{cases} \tag{15}$$

To allow for non monotonic loading, the crack density in (15) is only temporary, and any prior accumulated crack density is kept as a state variable of the lamina in case the sign of the stress reverses. Equation (15) applies only to mode I. For mode II (shear), the cracks are always active.

As a result of crack closure, it is necessary to split the center lamina if it spans the midsurface. This is because one side may be active and the other inactive under flexure. However, the COD are a function of the ply thickness, thus accounting for insitu effects. For example, under membrane tensile deformation, the COD in the center lamina of a $[0/90_2/0]$ is larger than in a $[0/90/90/0]$. To solve this problem, the code tests whether or not there is crack closure on either side of the midsurface in the center lamina. If there is, the laminate is analyzed with a split center lamina. Otherwise, the laminate is reanalyzed without split.

7 Resistance Curve

To obtain a better correlation between the model predictions and experimental results, the *mode I* ERR is corrected for in–situ resistance curve (R–curve) behavior. According to Griffith principle of classical fracture mechanics, the critical energy release rate for crack propagation G_c is a constant material property. However, for the case of crack multiplication in laminated composites, G_c increases with crack density λ, i.e., $G_c = G_c(\lambda)$ [18, 36, 72–75]. This phenomenon is called the *R–curve* behavior. Moreover, the crack growth resistance G_c also features ply thickness dependence, $G_c = G_c(\lambda, t)$. Both the critical ERR at damage initiation (G_c at $\lambda = 0$) and the subsequent slope of the $G_c = G_c(\lambda)$ variation are function of the ply thickness t. This is called *in–situ R–curve* behavior.

The phenomenon of *in–situ R–curve* behavior is attributed to fiber bridging during matrix cracking [61–66]. However, the micromechanics of fiber bridging, and consequently the phenomenological modeling of R–curve behavior is different for UD laminae and multidirectional laminates. While exponential equations were used in [67, 68], a linear R–curve model is proposed in this work. Due to lack of experimental data, *mode II* ERR is not corrected for the in–situ R-curve behavior. Thus, a constant value of G_{IIc}, independent of ply thickness and crack density, is used.

The resistance behavior, i.e., the variation of *mode I* ERR with crack density, at the reference ply thickness $t = t_{ref}$ is modeled by the following proposed equation

$$G_{Ic}^{ref} = G_{Ic,0}^{ref} + \tan(\beta_\lambda^{ref})\lambda \tag{16}$$

where $\lambda = \rho/t$ is the dimensional crack density, i.e., number of cracks per unit distance; t_{ref} is the thickness of the cracking lamina in the experiment, $G_{Ic,0}^{ref}$ is the mode I ERR at t_{ref}, and β_λ^{ref} is an adjustable parameter chosen to help correlate the *evolution* of cracking when the thickness of the cracking lamina is t_{ref}.

For lamina thickness different from t_{ref}, the insitu effect on the onset value of the critical ERR, namely $G_{Ic,0}$, is approximated by the following proposed equation

$$G_{Ic,0}(t) = G_{Ic,0}^{ref} \cdot \left[1 + (t/t_{ref} - 1)\left(\beta_0^t - 1\right)\right] \tag{17}$$

where β_0^t is an adjustable parameter, this time to help correlate the *initiation* of cracking at different ply thicknesses.

Finally, the variation of mode I ERR is modeled by the following proposed equation

$$G_{Ic}(\lambda, t) = G_{Ic,0}(t) + \left[1 + (t/t_{ref} - 1)\left(\beta_\lambda^t - 1\right)\right] \cdot \tan(\beta_\lambda^{ref}) \cdot \lambda \tag{18}$$

where β_λ^t is an adjustable parameter, this time to help correlate the *evolution* of cracking at different ply thicknesses.

8 Results

First, model predictions are shown for the common case of symmetric laminates subjected to membrane deformation. Experimental data for Carbon-Epoxy *T300/934* laminates is reported in [44, 69–71]. The thermoelastic properties of individual laminae are: $E_1 = 163.4 \ GPa$, $E_2 = 11.9 \ GPa$, $G_{12} = 6.5 \ GPa$, $\nu_{12} = 0.3$, $\nu_{23} = 0.5$, $\alpha_1 = 0.35 \cdot 10^{-6} \ ^oC$, $\alpha_2 = 28.8 \cdot 10^{-6} \ ^oC$, ply thickness $t_k = 0.132 \ mm$, and stress free temperature $SFT = 150 \ ^oC$.

The laminates include $[\pm 25/90_n]_S$ and $[0_m/90_n]_S$ for various values of m, n, which are reported in the figure captions. The loading is uniaxial extension ϵ_x.

A $[\pm 25/90_2]_S$ laminate is used to adjust the parameters in (16) and $[\pm 25/90_4]_S$ is used to adjust parameters in (17)–(18), yielding: $G_{IC,0}^{ref} = 0.2 \ N/mm$, $\beta_\lambda^{ref} = 6 \ deg.$, $\beta_0^t = 1.2$, $\beta_\lambda^t = 2$. Since matrix cracking takes place only in mode I, the value of the critical ERR for mode II, namely $G_{II,C}$, is irrelevant for this particular set of experimental data.

Model prediction of matrix cracking onset and evolution are compared against experimental results in Fig. 2–5, for various thicknesses of the cracking 90 ply stack in the $[\pm 25/90_n]_S$ laminates. Model predictions are in good agreement with experimental data for different thicknesses of the 90_n cracking stack. The expected trend of earlier damage initiation in the thicker plies is confirmed by both experimental and analytical results.

Two additional Carbon-Epoxy systems, AS4/Hercules 3501-6 and IM6/Avimid-K, with laminate stacking sequence (LSS) $[0_m/90_n]_S$ are evaluated using the experimental data presented in [9,10]. The values of m, n, are given in the figure captions. The loading case is uniaxial extension ϵ_x.

For *AS4/Hercules 3501-6*, the thermoelastic properties of the laminae are: $E_1 = 130 \ GPa$, $E_2 = 9.7 \ GPa$, $G_{12} = 5 \ GPa$, $\nu_{12} = 0.3$, $\nu_{23} = 0.5$, $\alpha_1 = -0.09 \cdot 10^{-6} \ ^oC$, $\alpha_2 = 28.8 \cdot 10^{-6} \ ^oC$, ply thickness $t_k = 0.125 \ mm$, and stress free temperature $SFT = 125^oC$.

The $[0/90]_S$ laminate is used to adjust the parameters in (16) and $[0/90_2]_S$ is used to adjust parameters in (17)–(18), yielding: $G_{IC,0}^{ref} = 0.14 \ N/mm$, $\beta_\lambda^{ref} = 1.5 \ deg.$, $\beta_0^t = 1.1$, $\beta_\lambda^t = 2$.

For *IM6/Avimid-K*, the thermoelastic properties of the laminae are: $E_1 = 134 \ GPa$, $E_2 = 9.8 \ GPa$, $G_{12} = 5.5 \ GPa$, $\nu_{12} = 0.3$, $\nu_{23} = 0.5$, $\alpha_1 = -0.09 \cdot 10^{-6} \ ^oC$, $\alpha_2 = 28.8 \cdot 10^{-6} \ ^oC$, ply thickness $t_k = 0.125 \ mm$, and stress free temperature $SFT = 225^oC$.

The $[0/90_2]_S$ laminate is used to adjust the parameters in (16) and $[0/90_3]_S$ is used to adjust parameters in (17)–(18), yielding: $G_{IC,0}^{ref} = 0.53 \ N/mm$, $\beta_\lambda^{ref} = 10 \ deg.$, $\beta_0^t = 1$, $\beta_\lambda^t = 1.4$.

Since matrix cracking takes place only in mode I, the value of the critical ERR for mode II, namely $G_{II,C}$, is irrelevant for these laminates and loading cases.

Crack density vs. stress is shown Fig. 6 for *AS4/Hercules 3501-6* and Fig. 7 for *IM6/Avimid-K*. The effect of the cracking ply thickness can be assessed by observing the set $[0_m/90_n]_S$ with m fixed and n variable. On the other hand, the constraining effect of the neighboring plies can be assessed by observing the set $[0_m/90_n]_S$ with n fixed and m variable.

Good correlation between model predictions and experimental data for both damage onset and damage progression for *AS4/Hercules 3501-6* is observed in Fig. 6. Some differences between predicted and the experimental values appear at high values of crack density λ, where the model predicts a steeper increase in crack density than the experimental data.

The thickness effect of the cracking ply shown in Fig. 6 is predicted well by the model. The constraining effect of the neighboring plies can be observed in Fig. 6 comparing the damage curves corresponding to $[0/90_2]_S$ and $[0_2/90_2]_S$ laminate configurations. Damage initiates earlier in the $[0/90_2]_S$ laminate featuring a thinner 0 neighboring ply than in the $[0_2/90_2]_S$ laminate. The same observations and comments apply to *IM6/Avimid-K*.

To illustrate the performance of the model when bending deformations are included, a number of laminates made of E-glass-Epoxy Fiberdux 913G-E-5-30% are evaluated. The laminate configurations and loading cases are:

- $[0/90_n/0]$ featuring cracks in the 90_n ply stack under uniaxial extension loading ϵ_x,

- $[0_n/90_n/+45_n/-45_n]_S$ and $[0_n/+45_n/-45_n]_S$ featuring cracks in the 90_n, $+45_n$, and -45_n stacks under uniaxial extension loading ϵ_x,

- $[90_n/0_n/-45_n/+45_n]_S$ under uniaxial bending κ_x.

The material is Glass/Epoxy *Fibredux 913G-E-5-30%* with the following thermo-elastic properties [36]: $E_1 = 34\ GPa$, $E_2 = 18\ GPa$, $G_{12} = 7.9\ GPa$, $\nu_{12} = 0.29$, $\nu_{23} = 0.41$, $\alpha_1 = 6.72 \cdot 10^{-6}\ {}^oC$, $\alpha_2 = 29.3 \cdot 10^{-6}\ {}^oC$, ply thickness $t_k = 0.125\ mm$, and stress free temperature $SFT = 125^oC$.

The $[0/90/0]$ laminate was used to adjust the parameters in (16), and $[0/90_2/0]$ was used to adjust the parameters in (17)–(18), yielding: $G_{IC,0}^{ref} = 0.2\ N/mm$, $\beta_\lambda^{ref} = 0$ deg., $\beta_0^t = 1, \beta_\lambda^t = 1$. Since the experimental data set includes laminate configurations such as $[0_n/90_n/+45_n/-45_n]_S$, featuring cracks in off–axis plies under mixed mode loading, the value of mode II critical ERR is assumed to be $G_{II,C} = 1\ N/mm$.

A set of experimental results is available in [36] for the $[0/90_n/0]$ LSS under uniaxial extension ϵ_x. Reduced laminate modulus are presented in Fig. 8 for various laminates. Good agreement between model predictions and experimental data can be noticed. Evolution of crack density vs. strain curves are presented in Fig. 9–12. The comparison to experimental data is very good for 90 and 90_2 cracking plies, but only satisfactory for 90_4 and 90_8 thicknesses at high crack densities. The observed discrepancy is may be caused by thicker plies being more prone to delamination induced by intralaminar transverse matrix cracking. In this case, part of the stored deformation energy is released for the formation of delamination damage, while the available energy for intra-laminar matrix cracking is reduced, thus explaining the analytical model predicting higher crack densities for thicker plies than reported by the experimental results. The delamination mechanism is not accounted for in the present model, thus being a limitation of the present model when delamination occurs simultaneously or as a result of intralaminar matrix cracks.

Additional experimental data, including flexural deformation κ_x under displacement control, is available for the $[90_2/0_2/-45_2/45_2]_S$ and $[90_2/-45_2/45_2]_S$ laminates. Matrix cracking was recorded at the surface ply, on the extension side of the bending specimen [36]. Comparison between predicted and experimental bending moment–curvature plots are presented in Fig. 13, where good agreement between predictions and experiments can be observed.

It is nevertheless true that, due to experimental setup difficulties, the matrix cracking experimental data for flexural deformation are very scarce in the literature, and for asymmetric LSS are inexistent, at the best of the author's knowledge. However, the predictive capabilities of the analytical model for these two situations can be assessed and compared against the expected trends by considered an initially symmetric LSS and comparing the damage evolution results for the case of pure extension ϵ_x, pure bending κ_x, and simultaneous extension–bending $\epsilon_x - \kappa_x$ (a loading ratio of $\kappa_x = 0.5 \cdot \epsilon_x$ is considered for the last case). The reason why a symmetric LSS can be used to test the ability of the model to treat asymmetric LSS's is that the symmetry of the laminate is lost in the moment of the matrix cracking initiation under flexural deformation. This is due to the fact that under bending loading matrix cracking is induced only in the tension plies, which triggers a stiffness reduction only for these plies, and consequently the material loses its symmetry. The LSS considered for this study, selected such that to provide relevant information regarding the predictive capabilities of the analytical model, is $[0/90_2^{(1)}/0/90_3^{(1)}/0_2/90_2^{(2)}/0/90_3^{(2)}/0]$. The superscripts (1) denotes plies at the bottom of the LSS (under compression for pure bending deformation), and the superscripts (2) denotes plies at the top of the LSS (under tension for pure bending deformation). The following Glass–Epoxy material system is considered: $E_1 = 35\ GPa$; $E_2 = 9\ GPa$; $G_{12} = 4\ GPa$; $\nu_{12} = 0.28$; $\nu_{23} = 0.42$, $\alpha_1 = 6.7 \cdot 10^{-6}\ {}^oC^{-1}$; $\alpha_2 = 29.3 \cdot 10^{-6}\ {}^oC^{-1}$, $G_{IC} = 0.20\ N/mm, G_{IIC} = 1\ N/mm$, ply thickness $t_k = 0.125\ mm$, and stress free temperature $SFT = 130\ {}^oC$. The in–situ R–curve fracture toughness behavior is not considered for this case.

The damage process for the extension loading is presented in Fig. 14, for bending loading is presented in Fig. 15, and for combined bending-extension loading is presented in Fig. 16. It can

be observed that, for extension loading case, matrix cracking first initiates in the thicker 90_3 ply, and then in the thinner 90_2 ply, this model prediction being according with the expected physical behavior of the material. Also as expected, the damage process in the top 90_2 and 90_3 plies (on the symmetric part of the laminate) is identical to the bottom 90_2 and 90_3 plies. The cracking process in one of the 0 plies is additionally plotted in Fig. 14, which shown no matrix cracking during extension loading, as expected.

On the contrary, for bending loading case damage initiates first in the thinner 90_2 ply, and then in the thicker 90_3 ply. This is because of the outer position of the 90_2 ply inside of the laminate under bending deformation, which translates in higher ply strain for the same applied curvature κ on the laminate. According with the expected behavior of the damage process, matrix cracking is not triggered at all in the mirror 90_2 and 90_3 plies, due to the fact that these plies are under compressive strain.

For the combined extension–bending loading case the cracking process initiates almost simultaneous in the top $90_2^{(2)}$ and $90_3^{(2)}$ plies. It is interesting at this moment to make a qualitative comparison with the damage onset for the cases of separate extension and separate bending presented in Fig. 14 and Fig. 15, respectively. For the pure extension case in Fig. 14 damage initiated first in the 90_3 plies followed by the 90_2 plies, due to the thickness effect of the cracking plies. For the pure bending case in Fig. 15 damage initiated first in the outer $90_2^{(2)}$ ply followed by the $90_3^{(2)}$ ply, due to the position of the plies inside of the laminate under bending. A combination of the two effects can be noticed in Fig. 16 for the combined extension–bending deformation, when damage in the top plies initiates almost simultaneous.

Regarding the damage process in the bottom $90_2^{(1)}$ and $90_3^{(1)}$ plies, it can be observed that there is matrix cracking in the $90_3^{(1)}$ ply, and there is no matrix cracking in the $90_2^{(1)}$ ply. Even if the bottom plies experience negative strains due to the bending deformation, they also experience positive strain due to the extension deformation. This combination is more dominated by the extension deformation for the $90_3^{(1)}$ ply, and it is more dominated by the bending deformation for the $90_2^{(1)}$, because of the position these plies have inside of the laminate. This is the reason why matrix cracking appears in the $90_3^{(1)}$ ply and it does not appear in the $90_2^{(1)}$ ply.

9   Conclusions

The multiple aspects that influence transverse damage onset and evolution (growth) in laminated composites subject to membrane and flexural deformations are accounted in this work. Comparison of model predictions to experimental data are quite good. The effect of clustering, both on the cracking lamina and on the supporting laminate, as well as the effect of the laminate stacking sequence (LSS) are captured adequately, with the model providing the expected trends. Significant R-curve behavior is noticed when the experimental data is compared to the model results. The choice of damage variable, namely crack density, is fortunate in that it allows to adjust the model parameters with experimental data in the form of crack density rather than modulus reduction; the later being difficult to detect for Carbon-Epoxy composites.
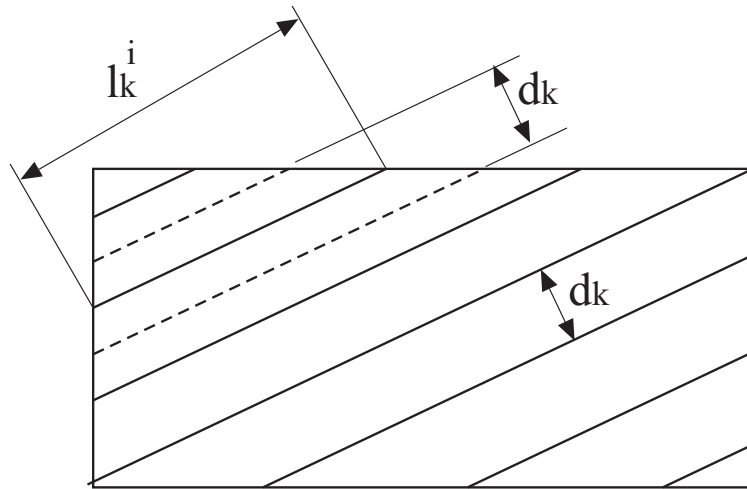
Figure 1: An equally spaced pattern of matrix cracks in one lamina of a laminate.
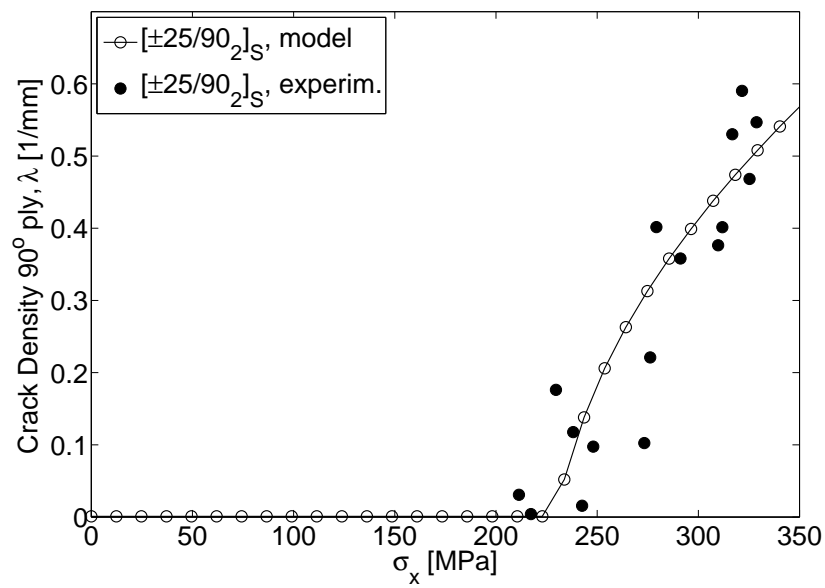
Figure 2: Predicted matrix cracking evolution compared to experimental data [70, 71] for $[\pm 25/90_2]_S$.
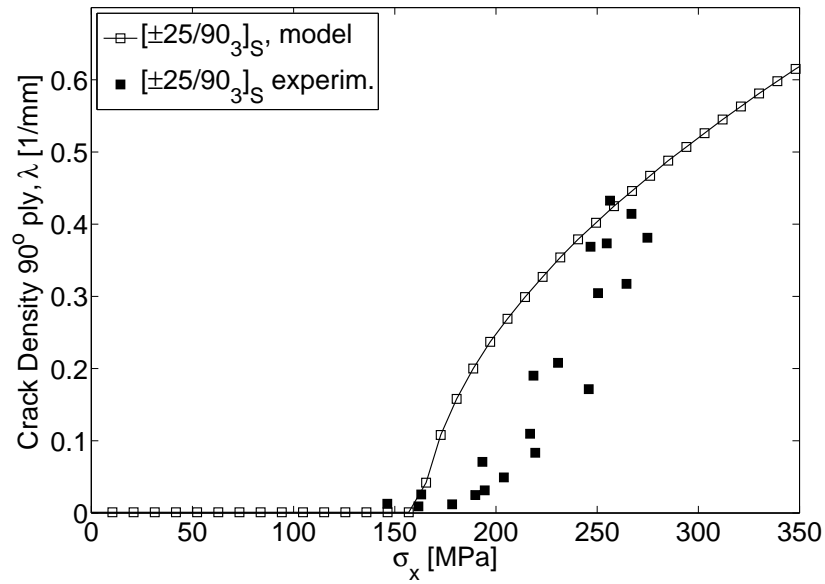
Figure 3: Predicted matrix cracking evolution compared to experimental data [70, 71] for $[\pm 25/90_3]_S$.
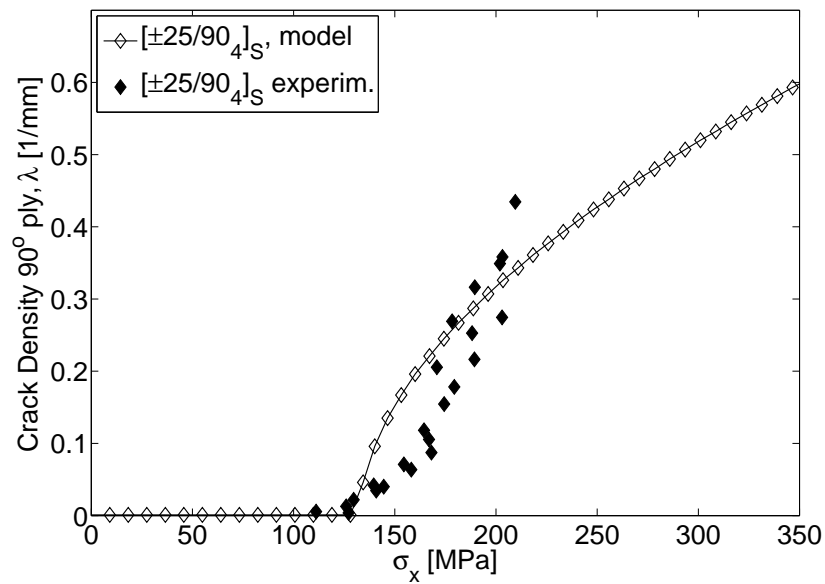
Figure 4: Predicted matrix cracking evolution compared to experimental data [70, 71] for $[\pm 25/90_4]_S$.
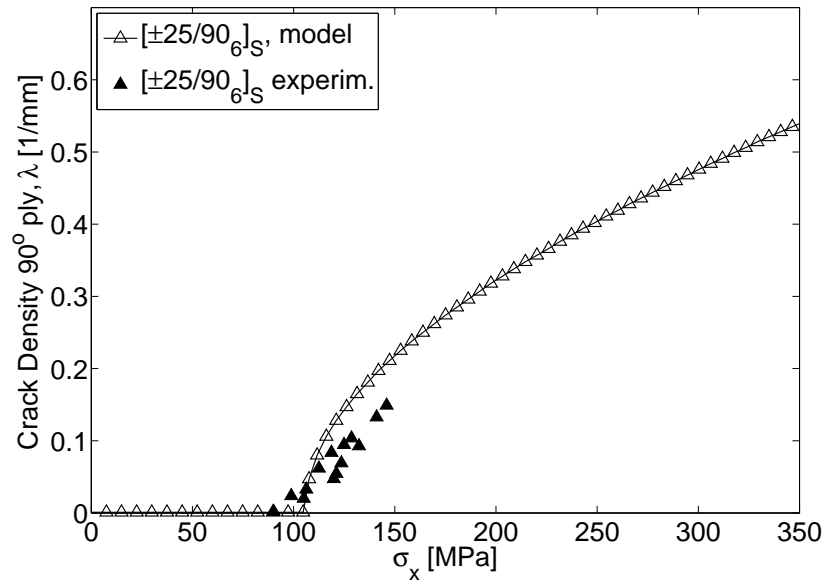
Figure 5: Predicted matrix cracking evolution compared to experimental data [70, 71] for $[\pm 25/90_6]_S$.
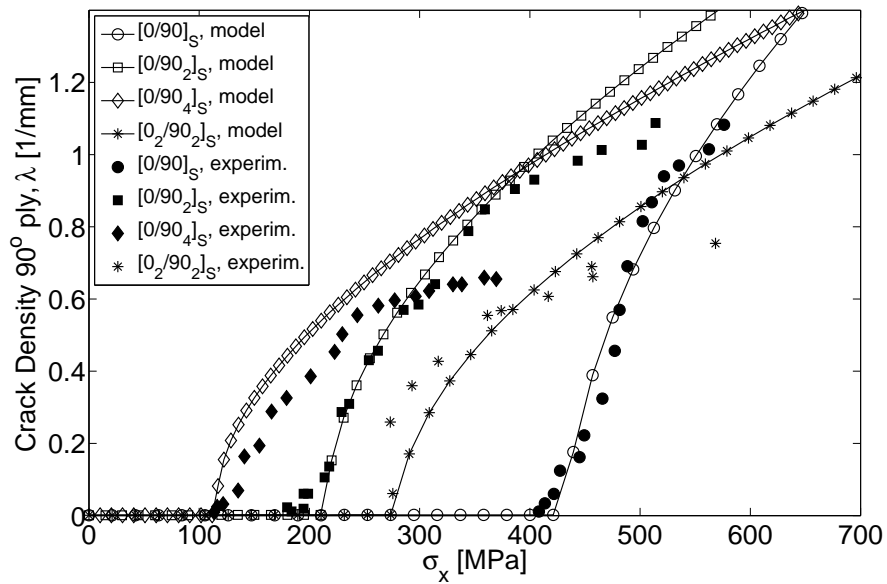
Figure 6: Predicted matrix cracking evolution compared to experimental data [9,10] for $[0_m/90_n]_S$ AS4/Hercules 3501-6.
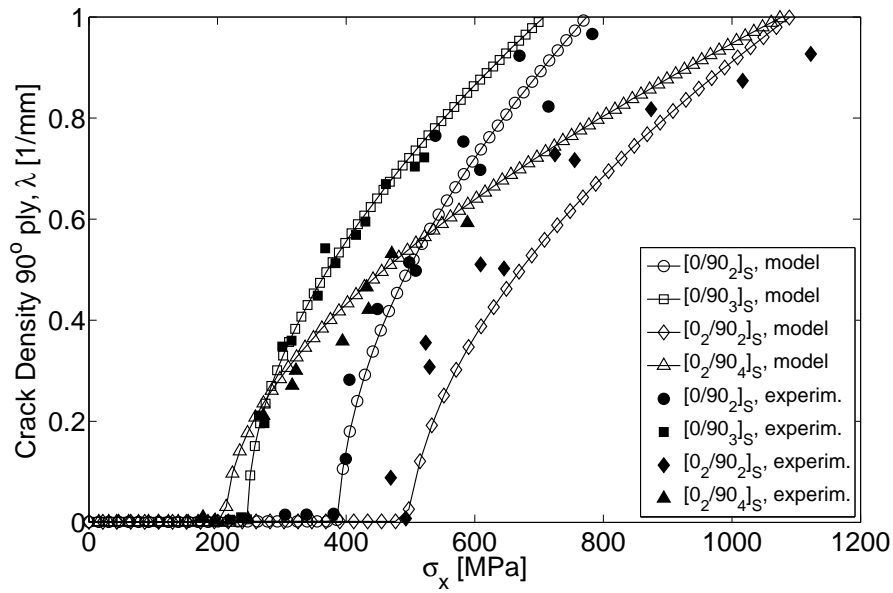
Figure 7: Predicted matrix cracking evolution compared to experimental data [9, 10] for $[0_m/90_n]_S$ IM6/Avimid-K.
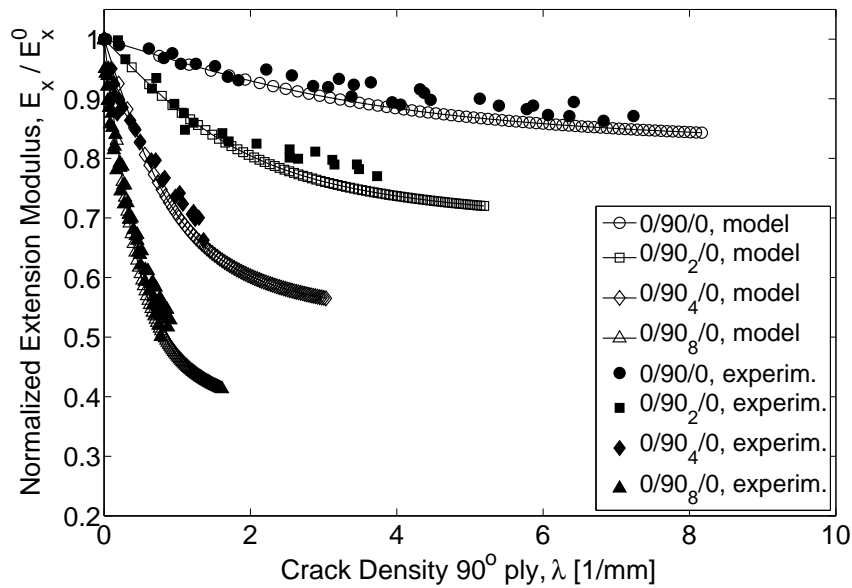
Figure 8: Predicted Young modulus compared to experimental data [36] for $[0/90_n/0]$ under ϵ_x loading.
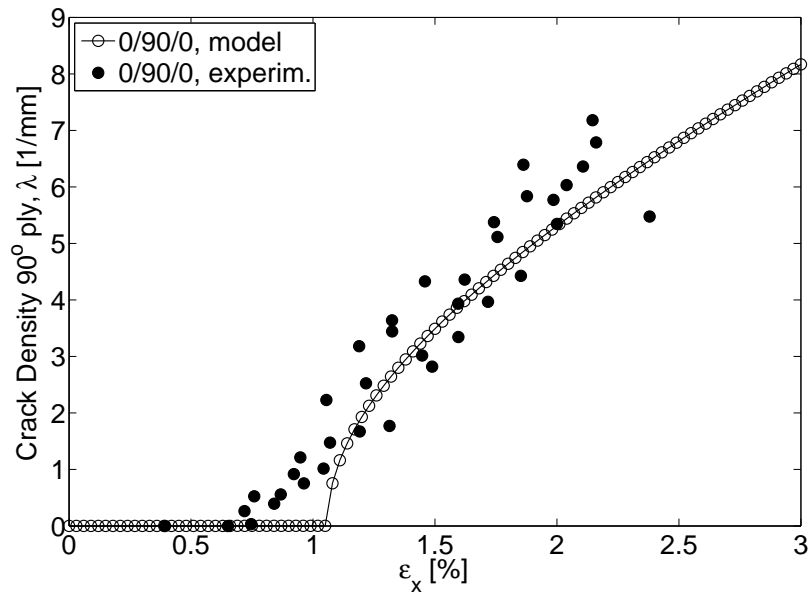
Figure 9: Predicted matrix cracking evolution compared to experimental data [36] for $[0/90/0]$ under ϵ_x loading.
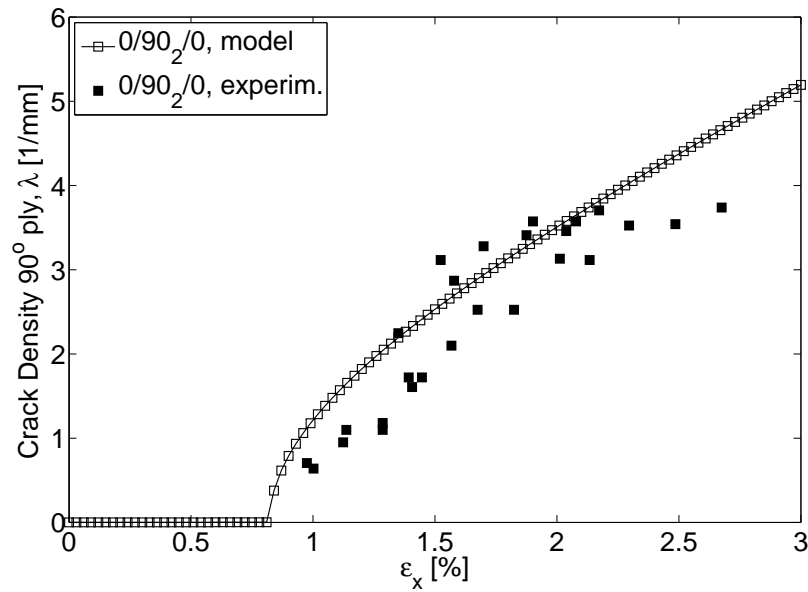
Figure 10: Predicted matrix cracking evolution compared to experimental data [36] for $[0/90_2/0]$ under ϵ_x loading.
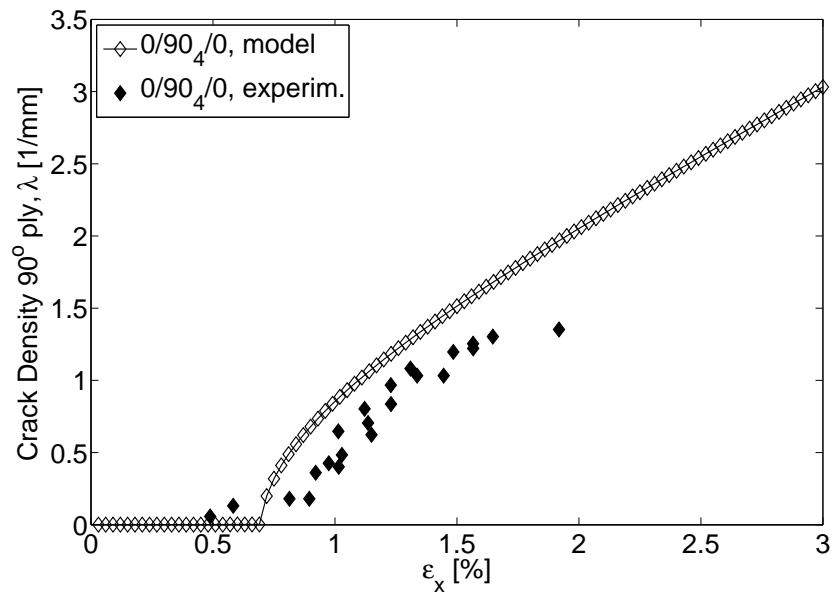
Figure 11: Predicted matrix cracking evolution compared to experimental data [36] for $[0/90_4/0]$ under ϵ_x loading.
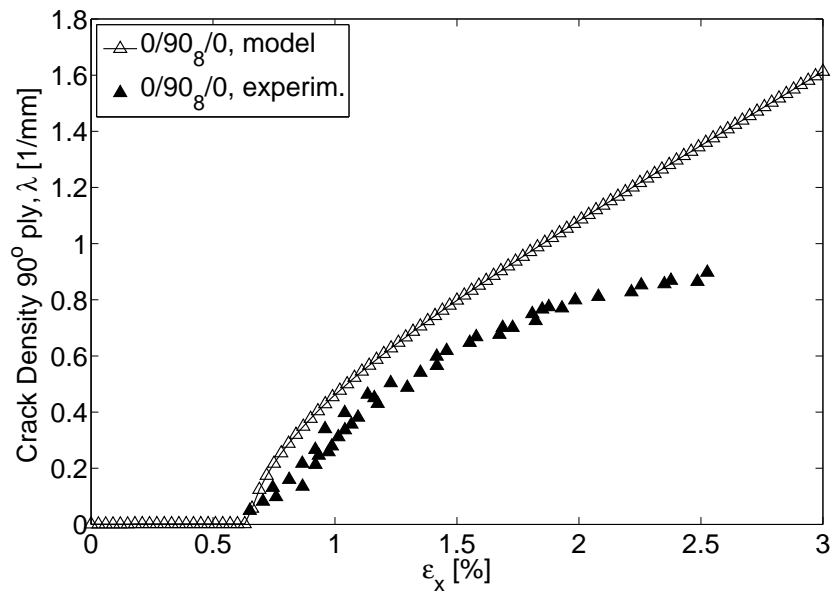
Figure 12: Predicted matrix cracking evolution compared to experimental data [36] for $[0/90_8/0]$ under ϵ_x loading.
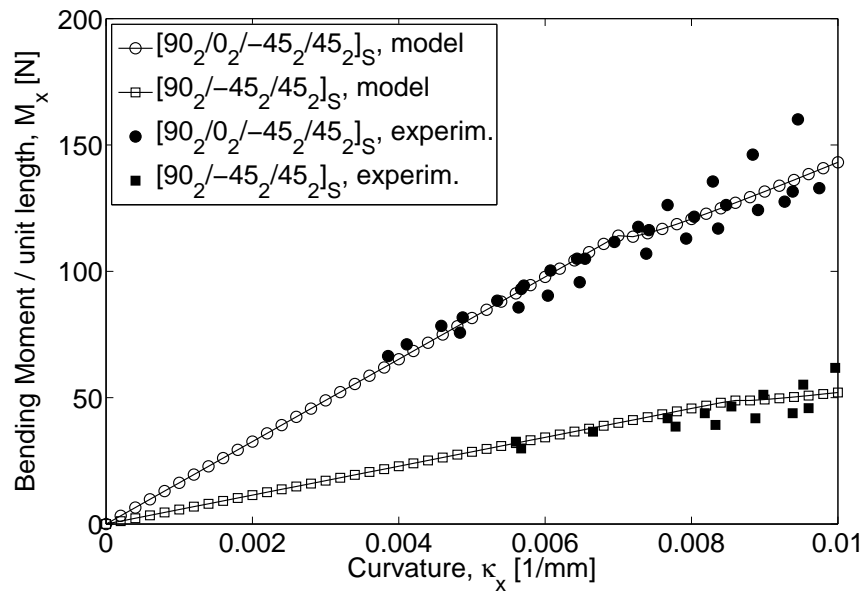
Figure 13: Predicted moment-curvature evolution compared to experimental data [36] for $[90_2/0_2/-45_2/+45_2]_S$ and $[90_2/-45_2/+45_2]_S$ under flexural loading κ_x.
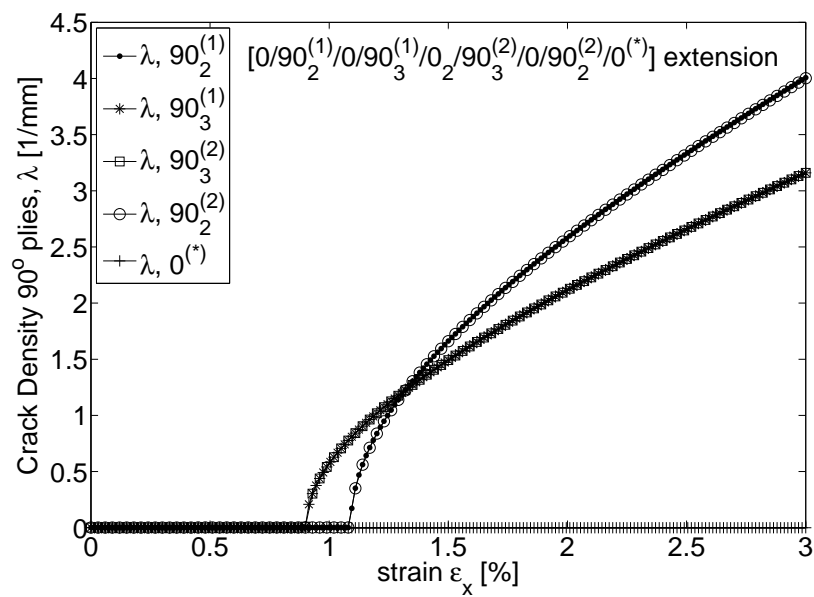
Figure 14: Damage evolution under extension loading, $\lambda = \lambda(\epsilon_x)$.
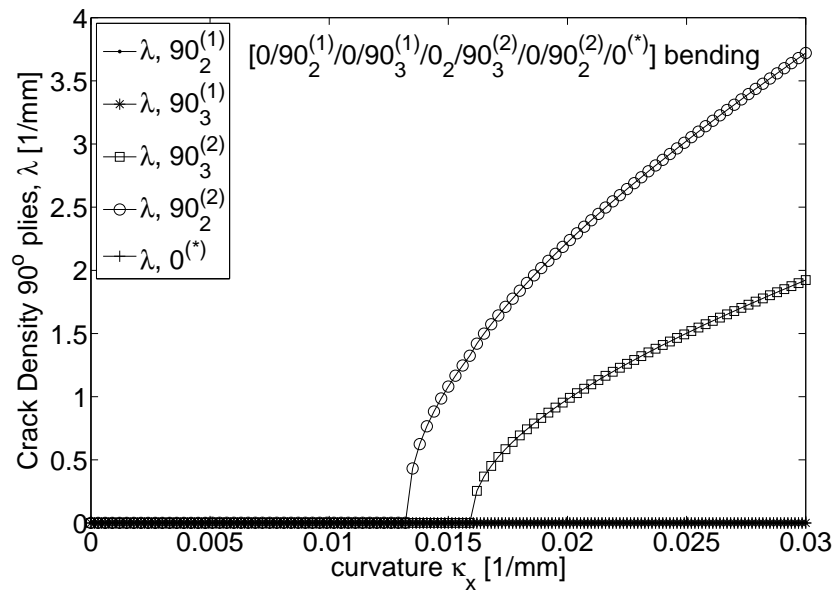
Figure 15: Damage evolution under bending loading, $\lambda = \lambda(\kappa_x)$.
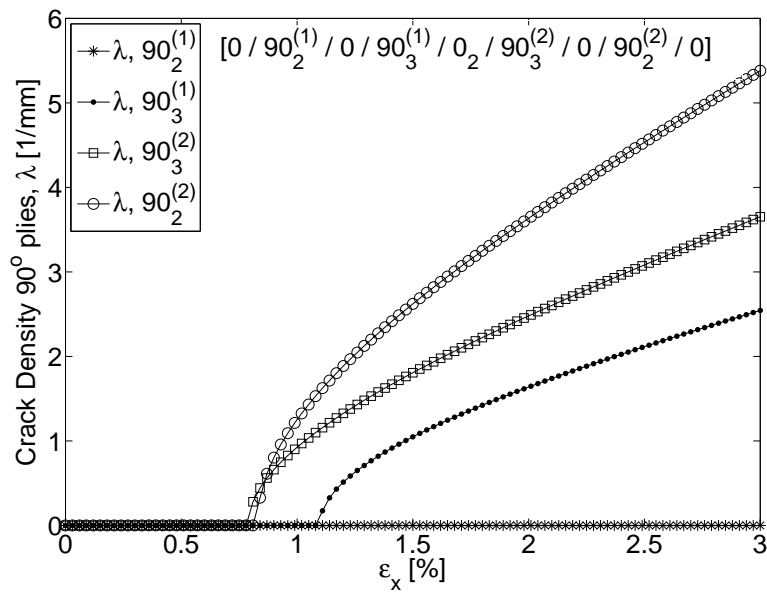
Figure 16: Damage process for the case of extension–bending combined loading, $(\epsilon_x - \kappa_x)$.

References

[1] S. E. Groves, C. E. Harris, A. L. Highsmith, D. H. Allen, and R. G. Norvell. Experimental and analytical treatment of matrix cracking in cross-ply laminates. *Experimental Mechanics*, 27(1):73–79, 1987.

[2] D. H. Allen, C. E. Harris, and S. E. Groves. A thermomechanical constitutive theory for elastic composites with distributed damage - II. application to matrix cracking in laminated composites. *International Journal of Solids and Structures*, 23(9):1319–38, 1987.

[3] S. Li, S. R. Reid, and P. D. Soden. Modelling the damage due to transverse matrix cracking in fiber-reinforced laminates. In *Proc. 2nd Int. Conf. on Nonlinear Mechanics (ICNP-2)*, pages 320–323. Peking University Press, 1993.

[4] S. Li, S. R. Reid, and P. D. Soden. A continuum damage model for transverse matrix cracking in laminated fibre-reinforced composites. *Philosophical Transactions of the Royal Society London, Series A (Mathematical, Physical and Engineering Sciences)*, 356(1746):2379–412, 10/15 1998.

[5] J. Varna, R. Joffe, N. V. Akshantala, and R. Talreja. Damage in composite laminates with off-axis plies. *Composites Science and Technology*, 59(14):2139–2147, 1999.

[6] Janis Varna, Roberts Joffe, and Ramesh Talreja. A synergistic damage-mechanics analysis of transverse cracking $[\pm\theta/90_4]s$ laminates. *Composites Science and Technology*, 61(5):657–665, 2001.

[7] Ever J. Barbero and Liliana De Vivo. Constitutive model for elastic damage in fiber-reinforced pmc laminae. *International Journal of Damage Mechanics*, 10(1):73–93, 2001.

[8] J. A. Nairn and S. Hu. *Damage Mechanics of Composite Materials*, volume 9 of *Composite Materials Series*, chapter Matrix Microcracking, pages 187–244. Elsevier, 1994.

[9] S. Liu and J. A. Nairn. The formation and propagation of matrix microcracks in cross-ply laminates during static loading. *Journal of Reinforced Plastics and Composites*, 11(2):158–78, 02 1992.

[10] J. A. Nairn. *Polymer Matrix Composites*, volume 2 of *Comprehensive Composite Materials*, chapter Matrix Microcracking in Composites, pages 403–432. Elsevier Science, 2000.

[11] J. A. Nairn. The strain energy release rate of composite microcracking: a variational approach. *Journal of Composite Materials*, 23(11):1106–29, 11 1989.

[12] J. A. Nairn, S. Hu, S. Liu, and J. S. Bark. The initiation, propagation, and effect of matrix microcracks in cross-ply and related laminates. In *Proc. of the 1st NASA Advanced Comp. Tech. Conf.*, pages 497–512, Oct. 29 - Nov. 1, 1990 1990.

[13] J. A. Nairn. Microcracking, microcrack-induced delamination, and longitudinal splitting of advanced composite structures. Technical Report NASA Contractor Report 4472, 1992.

[14] J. A. Nairn. Applications of finite fracture mechanics for predicting fracture events in composites. In *5th Int'l Conf. on Deform. and Fract. of Comp.*, 18-19 March 1999.

[15] J. A. Nairn. Fracture mechanics of composites with residual stresses, imperfect interfaces, and traction-loaded cracks. In *Workshop 'Recent Advances in Continuum Damage Mechanics for Composites'*, volume 61, pages 2159–67, UK, 20-22 Sept. 2000. Elsevier.

[16] J. A. Nairn and D. A. Mendels. On the use of planar shear-lag methods for stress-transfer analysis of multilayered composites. *Mechanics of Materials*, 33(6):335–362, 2001.

[17] J. A. Nairn. *Finite Fracture Mechanics of Matrix Microcracking in Composites*, pages 207–212. Application of Fracture Mechanics to Polymers, Adhesives and Composites. Elsevier, 2004.

[18] Y. M. Han, H. T. Hahn, and R. B. Croman. A simplified analysis of transverse ply cracking in cross-ply laminates. *Composites Science and Technology*, 31(3):165–177, 1988.

[19] C. T. Herakovich, J. Aboudi, S. W. Lee, and E. A. Strauss. Damage in composite laminates: Effects of transverse cracks. *Mechanics of Materials*, 7(2):91–107, 11 1988.

[20] J. Aboudi, S. W. Lee, and C. T. Herakovich. Three-dimensional analysis of laminates with cross cracks. *Journal of Applied Mechanics, Transactions ASME*, 55(2):389–397, 1988.

[21] F. W. Crossman, W. J. Warren, A. S. D. Wang, and G. E. Law. Initiation and growth of transverse cracks and edge delamination in composite laminates. ii - experimental correlation. *Journal of Composite Materials Suplement*, 14(1):88–108, 1980.

[22] D. L. Flaggs and M. H. Kural. Experimental determination of the in situ transverse lamina strength in graphite/epoxy laminates. *Journal of Composite Materials*, 16:103–16, 03 1982.

[23] S. H. Lim and S. Li. Energy release rates for transverse cracking and delaminations induced by transverse cracks in laminated composites. *Composites Part A*, 36(11):1467–1476, 2005.

[24] S. Li and F. Hafeez. Variation-based cracked laminate analysis revisited and fundamentally extended. *International Journal of Solids and Structures*, 46(20):3505–3515, 2009.

[25] J. L Rebiere and D. Gamby. A decomposition of the strain energy release rate associated with the initiation of transverse cracking, longitudinal cracking and delamination in cross-ply laminates. *Composite Structures*, 84(2):186–197, 2008.

[26] S. C. Tan and R. J. Nuismer. A theory for progressive matrix cracking in composite laminates. *Journal of Composite Materials*, 23(10):1029–47, 10 1989.

[27] R. J. Nuismer and S. C. Tan. Constitutive relations of a cracked composite lamina. *Journal of Composite Materials*, 22(4):306–21, 04 1988.

[28] T. Yokozeki and T. Aoki. Stress analysis of symmetric laminates with obliquely-crossed matrix cracks. *Advanced Composite Materials*, 13(2):121–40, 2004.

[29] T. Yokozeki and T. Aoki. Overall thermoelastic properties of symmetric laminates containing obliquely crossed matrix cracks. *Composites Science and Technology*, 65(11-12):1647–54, 2005.

[30] Z. Hashin. Analysis of cracked laminates: a variational approach. Mechanics of Materials, 4:121:136, 1985.

[31] J. Zhang, J. Fan, and C. Soutis. Analysis of multiple matrix cracking in $[\pm\theta/90_n]_s$ composite laminates, part I, inplane stiffness properties. Composites, 23(5) 291–304, 1992.

[32] P. Gudmundson and S. Ostlund. First order analysis of stiffness reduction due to matrix cracking. *Journal of Composite Materials*, 26(7):1009–30, 1992.

[33] P. Gudmundson and S. Ostlund. Prediction of thermoelastic properties of composite laminates with matrix cracks. *Composites Science and Technology*, 44(2):95–105, 1992.

[34] P. Gudmundson and W. Zang. An analytic model for thermoelastic properties of composite laminates containing transverse matrix cracks. *International Journal of Solids and Structures*, 30(23):3211–31, 1993.

[35] E. Adolfsson and P. Gudmundson. Thermoelastic properties in combined bending and extension of thin composite laminates with transverse matrix cracks. *International Journal of Solids and Structures*, 34(16):2035–60, 06 1997.

[36] E. Adolfsson and P. Gudmundson. Matrix crack initiation and progression in composite laminates subjected to bending and extension. *International Journal of Solids and Structures*, 36(21):3131–3169, 1999.

[37] W. Zang and P. Gudmundson. Damage evolution and thermoelastic properties of composite laminates. *International Journal of Damage Mechanics*, 2(3):290–308, 07 1993.

[38] E. Adolfsson and P. Gudmundson. Matrix crack induced stiffness reductions in [(0m/90n/+p/-q)s]m composite laminates. *Composites Engineering*, 5(1):107–23, 1995.

[39] P. Lundmark and J. Varna. Modeling thermo-mechanical properties of damaged laminates. In *3rd International Conference on Fracture and Damage Mechanics, FDM 2003*, volume 251-252 of *Advances in Fracture and Damage Mechanics*, pages 381–7, Switzerland, 2-4 Sept. 2003. Trans Tech Publications.

[40] M. Kachanov. volume 30 of *Advances in Applied Mechanics*, chapter Elastic solids with many cracks and related problems, pages 260–445. Academic Press, Inc., 1993.

[41] T. Yokozeki, T. Aoki, and T. Ishikawa. Transverse crack propagation in the specimen width direction of cfrp laminates under static tensile loadings. *Journal of Composite Materials*, 36(17):2085–99, 2002.

[42] T. Yokozeki, T. Aoki, and T. Ishikawa. Consecutive matrix cracking in contiguous plies of composite laminates. *International Journal of Solids and Structures*, 42(9-10):2785–802, 05 2005.

[43] T. Yokozeki, T. Aoki, T. Ogasawara, and T. Ishikawa. Effects of layup angle and ply thickness on matrix crack interaction in contiguous plies of composite laminates. *Composites Part A (Applied Science and Manufacturing)*, 36(9):1229–35, 2005.

[44] A. S. D. Wang, P. C. Chou, and S. C. Lei. A stochastic model for the growth of matrix cracks in composite laminates. *Journal of Composite Materials*, 18(3):239–54, 05 1984.

[45] D. H. Cortes and E. J. Barbero. Stiffness reduction and fracture evolution of oblique matrix cracks in composite laminates. *Annals of Solids and Structural Mechanics*, 1(1):29–40, 2010.

[46] E. J. Barbero and D. H. Cortes. A mechanistic model for transverse damage initiation, evolution, and stiffness reduction in laminated composites. *Composites Part B*, 41:124–132, 2010.

[47] P. A. Smith and S. L. Ogin. Characterization and modelling of matrix cracking in a (0/90)2s gfrp laminate loaded in flexure. *Proceedings of the Royal Society of London, Series A (Mathematical, Physical and Engineering Sciences)*, 456(2003):2755–70, 11/08 2000.

[48] P. A. Smith and S. L. Ogin. On transverse matrix cracking in cross-ply laminates loaded in simple bending. *Composites Part A: Applied Science and Manufacturing*, 30(8):1003–1008, 1999.

[49] S. Kuriakose and R. Talreja. Variational solutions to stresses in cracked cross-ply laminates under bending. *International Journal of Solids and Structures*, 41(9-10):2337–47, 05 2004.

[50] S. Li, S. R. Reid, and P. D. Soden. A finite strip analysis of cracked laminates. *Mechanics of Materials*, 18(4):289–311, 10 1994.

[51] C. G. Davila, P. P. Camanho, and C. A. Rose. Failure criteria for frp laminates. *Journal of Composite Materials*, 39(4):323–345, 2005.

[52] H. T. Hahn. A mixed-mode fracture criterion for composite materials. *Composites Technology Review*, 5:26–29, 1983.

[53] J. A. Mayugo, P. P. Camanho, P. Maimi, and C. G. Dávila. Analytical modeling of transverse matrix cracking of $[\pm\theta/90_n]$ composite laminates under multiaxial loading. *Mechanics of Advanced Materials and Structures*, 17:237–45, 2010.

[54] E. J. Barbero. *Finite Element Analysis of Composite Materials*. Taylor & Francis, 2007.

[55] E. J. Barbero, G. Sgambitterra, A. Adumitroaie, and X. Martinez. A discrete constitutive model for transverse and shear damage of symmetric laminates with arbitrary stacking sequence. *Composite Structures*, 93(2):1021–30, 01 2011.

[56] G. Sgambitterra, A. Adumitroaie, E. J. Barbero, and A. Tessler. A robust three-node shell element for laminated composites with matrix damage. *Composites Part B: Engineering*, 42(1):41–50, 2011.

[57] P. Camanho and C. Davila. Mixed-mode decohesion finite elements for the simulation of delamination in composite materials. *NASA/TM-2002-211737*, pages 1–37, 2002.

[58] A. Parvizi, K. W. Garrett, and J. E. Bailey. Constrained cracking in glass fiber reinforced epoxy cross-ply laminates. *Journal of Materials Science*, 13:195–201, 1978.

[59] E. J. Barbero. *Introduction to Composite Materials Design–Second Edition*. CRC Press, Philadelphia, PA, 1st edition, 2010.

[60] H. Tada, P. C. Paris, and G. R. Irwin. *Stress Analysis of Cracks Handbook*. ASME Press, New York, NY, 3rd edition, 2000.

[61] K.D. Cowley and P.W.R. Beaumont. The interlaminar and intralaminar fracture toughness of carbon-fibre/polymer composites: the effect of temperature. *Composites Science and Technology*, 57(11):1433 – 1444, 1997.

[62] R.W. Truss, P.J. Hine, and R.A. Duckett. Interlaminar and intralaminar fracture toughness of uniaxial continuous and discontinuous carbon fibre/epoxy composites. *Composites Part A (Applied Science and Manufacturing)*, 28A(7):627 – 36, 1997//.

[63] U. Hansen and Jr. Gillespie, J.W. Dependence of intralaminar fracture toughness on direction of crack propagation in unidirectional composites. *Journal of Composites Technology and Research*, 20(2):89 – 99, 1998/04/.

[64] B.F. Sorensen and T.K. Jacobsen. Large-scale bridging in composites: R-curves and bridging laws. *Composites Part A (Applied Science and Manufacturing)*, 29A(11):1443 – 51, 1998.

[65] B. F. Sorensen and T. K. Jacobsen. Determination of cohesive laws by J integral approach. *Engineering Fracture Mechanics*, 70:1841–58, 2003.

[66] M. Iwamoto, Q.-Q. Ni, T. Fujiwara, and K. Kurashiki. Intralaminar fracture mechanism in unidirectional cfrp composites. part i: Intralaminar toughness and ae characteristics. *Engineering Fracture Mechanics*, 64(6):721 – 745, 1999.

[67] J. Zhang, J. Fan, and C. Soutis. Analysis of multiple matrix cracking in $[\pm\theta_m/90_n]s$ composite laminates. part I: In-plane stiffness properties. *Composites*, 23(5):291–298, September 1992.

[68] J. Fan and J. Zhang. In-situ damage evolution and micro/macro transition for laminated composites. *Composites Science and Technology*, 47:107–118, 1993.

[69] A. S. D. Wang. Fracture mechanics of sublaminate cracks in composite materials. *Composites Technology Review*, 6(2):45–62, 1984.

[70] F. W. Crossman, W. J. Warren, A. S. D. Wang, and G. E. Law. Initiation and growth of transverse cracks and edge delamination in composite laminates. ii - experimental correlation. *Journal of Composite Materials Suplement*, 14(1):88–108, 1980.

[71] F. W. Crossman and A. S. D. Wang. *Damage in Composite Materials*, chapter The dependence of transverse cracking and delamination on ply thickness in Graphite/Epoxy laminates, pages 118–139. ASTM International, 1982.

[72] J. Zhang, J. Fan, and C. Soutis Analysis of multiple matrix cracking in $[\pm\theta_m/90_n]s$ composite laminates. Part II: Development of transverse ply cracks *Composites*, 23(5):299–304, September 1992.

[73] D. T. G. Katerelos, J. Varna, and C. Galiotis Energy criterion for modeling damage evolution in cross-ply composite laminates *Composites Science and Technology*, 68:2318–24, 2008.

[74] S. Yalvac, L. D. Yats, and D. G. Wetters Transverse ply cracking in toughened and untoughened Graphyte/Epoxy and Graphyte/Polycyanate cross ply laminates *Journal of Composite Materials*, 25:1653–67, 1991.

[75] J. Fan and J. Zhang In-situ damage evolution and micro/macro transition for laminated composites *Composites Science and Technology*, 47:107–18, 1993.